Microscopic description of production cross sections including deexcitation effects

Kazuyuki Sekizawa*
Faculty of Physics, Warsaw University of Technology, Ulica Koszykowa 75, PL-00-662 Warsaw, Poland
(Received 24 May 2017; published 24 July 2017)

Background: At the forefront of the nuclear science, production of new neutron-rich isotopes is continuously pursued at accelerator laboratories all over the world. To explore the currently unknown territories in the nuclear chart far away from the stability, reliable theoretical predictions are inevitable.
Purpose: To provide a reliable prediction of production cross sections taking into account secondary deexcitation processes, both particle evaporation and fission, a new method called TDHF+GEMINI is proposed, which combines the microscopic time-dependent Hartree-Fock (TDHF) theory with a sophisticated statistical compound-nucleus deexcitation model, GEMINI++.
Methods: Low-energy heavy ion reactions are described based on three-dimensional Skyrme-TDHF calculations. Using the particle-number projection method, production probabilities, total angular momenta, and excitation energies of primary reaction products are extracted from the TDHF wave function after collision. Production cross sections for secondary reaction products are evaluated employing GEMINI++. Results are compared with available experimental data and widely used GRAZING calculations.
Results: The method is applied to describe cross sections for multinucleon transfer processes in ^{40}Ca + ^{124}Sn ($E_{\rm c.m.} \simeq 128.54$ MeV), ^{48}Ca + ^{124}Sn ($E_{\rm c.m.} \simeq 125.44$ MeV), ^{40}Ca + ^{208}Pb ($E_{\rm c.m.} \simeq 208.84$ MeV), ^{58}Ni + ^{208}Pb ($E_{\rm c.m.} \simeq 256.79$ MeV), ^{64}Ni + ^{238}U ($E_{\rm c.m.} \simeq 307.35$ MeV), and ^{136}Xe + ^{198}Pt ($E_{\rm c.m.} \simeq 644.98$ MeV) reactions at energies close to the Coulomb barrier. It is shown that the inclusion of secondary deexcitation processes, which are dominated by neutron evaporation in the present systems, substantially improves agreement with the experimental data. The magnitude of the evaporation effects is very similar to the one observed in GRAZING calculations. TDHF+GEMINI provides better description of the absolute value of the cross sections for channels involving transfer of more than one proton, compared to the GRAZING results. However, there remain discrepancies between the measurements and the calculated cross sections, indicating a limit of the theoretical framework that works with a single mean-field potential. Possible causes of the discrepancies are discussed.
Conclusions: To perfectly reproduce experimental cross sections for multinucleon transfer processes, one should go beyond the standard self-consistent mean-field description. Nevertheless, the proposed method will provide valuable information to optimize production mechanisms of new neutron-rich nuclei through its microscopic, nonempirical predictions.

DOI: 10.1103/PhysRevC.96.014615

I. INTRODUCTION

To expand our knowledge of the nature of the atomic nuclei, it is obviously important to produce new neutron-rich unstable isotopes that have not yet been produced to date, and study their properties both experimentally and theoretically. However, the optimal reaction condition, such as projectile-target combinations and incident energies, to produce such extremely unstable nuclei is not obvious, and reliable theoretical predictions are mandatory to guide experiments at current and future radioactive-ion beam facilities. This paper aims to provide a predictive model of production cross sections in low-energy heavy ion reactions.

To describe low-energy heavy ion reactions, various models have been developed. Semiclassical models, called GRAZING [1] and complex Wentzel-Kramers-Brillouin (CWKB) [2], have shown remarkable successes in describing multinucleon transfer (MNT) processes in peripheral collisions [3]. The GRAZING code was extended to include effects of transfer-induced fission in competition with particle evaporation [4]. A possible drawback of those models lies in insufficient description of deep-inelastic processes at small impact parameters. On the other hand, different theoretical approaches have also been developed: e.g., a dynamical model based on Langevin-type equations of motion [5–12], dinuclear system model (DNS) [13–28], and improved quantum molecular dynamics model (ImQMD) [29–38]. Although those models can describe both peripheral and damped collisions, including fusion and quasifission (QF) processes, they are to some extent empirical containing model parameters. To provide a reliable prediction to produce new neutron-rich isotopes, it is desirable to have as few adjustable parameters as possible. In the present paper, a method is developed to predict production cross sections based on a microscopic framework of the time-dependent Hartree-Fock (TDHF) theory.

The TDHF theory allows one to describe nuclear dynamics microscopically from nucleonic degrees of freedom. The theory itself was proposed in 1930 [39], and its application to nuclear systems already started about 40 years ago [40,41]. Since then, it was developed as an omnipotent tool, rooted with the time-dependent density functional theory (TDDFT), to study nuclear structure and dynamics in a unified way [42–45]. Recently, we have applied the theory to study MNT

*sekizawa@if.pw.edu.pl

and QF processes in various systems at energies around the Coulomb barrier [46–51]. Applying the particle-number projection (PNP) method [52], transfer cross sections were evaluated based on the TDHF theory. Comparisons with measured cross sections revealed that the theory, being with no adjustable parameters, can describe transfer cross sections quite well in accuracy comparable to the existing models [46]. However, the calculated cross sections were of primary (excited) reaction products which are to be deexcited through particle evaporation and/or fission. Because of this fact discrepancy arises when compared with experimental data, especially for channels accompanying transfer of many nucleons. The TDHF description of production cross sections was thus beset with the absence of deexcitation processes that limits its predictive power.

In this paper, a method, called TDHF+GEMINI, is proposed to cure the drawback of the TDHF description. Namely, secondary deexcitation processes of primary reaction products, both particle evaporation and fission, are simulated employing a state-of-the-art statistical model, GEMINI++ [53]. Those secondary processes are difficult to investigate within TDHF, because of, e.g., its much longer time scales. The inputs of statistical-model calculations, spin, and excitation energy of primary reaction products, are extracted from the TDHF wave function after collision, using an extended PNP method [47]. The method is applied to ^{40,48}Ca + ^{124}Sn, ^{40}Ca + ^{208}Pb, ^{58}Ni + ^{208}Pb, ^{64}Ni + ^{238}U, and ^{136}Xe + ^{198}Pt reactions for which measured cross sections are available. To demonstrate the accuracy of the proposed method is the main purpose of this work.

It was appreciated that TDHF provides valuable insight into complex many-body dynamics of low-energy heavy ion reactions. However, it works with a single mean-field potential which is deterministically associated with the initial condition. In other words, fluctuations in collective space are absent in the TDHF dynamics. Indeed, it was shown that the theory is optimized to describe the expectation value of one-body observables [42,54], and fluctuations of them are known to be severely underestimated [55–58]. How and to what extent beyond-mean-field fluctuations play a role in MNT reactions is an open question. Moreover, internucleon correlations are also not included in TDHF. Outcomes of MNT reactions may reflect effects of internucleon correlations, because of possible transfer of a correlated pair or a cluster of nucleons. Recently, it has become possible to pursue microscopic simulations of heavy ion reactions including the pairing correlations [59–66]. It should be noted here that the proposed method can, in principle, be extended to incorporate with the pairing correlations. In the present paper, however, we will focus on a treatment without pairing and leave further extension/application to include the pairing correlations as a future task. Nevertheless, it has to be noted here that, by extending the application of the theoretical framework based on the TDHF theory as far as possible, this work will shed light on the validity of the theoretical framework that works with a single mean-field potential, without internucleon correlations.

The article is organized as follows. In Sec. II, the methodology of TDHF+GEMINI is outlined. In Sec. III, numerical results for various reactions are presented and are compared with available experimental data. In Sec. IV, a summary of the present work is given.

II. TDHF+GEMINI

In this section, we focus on the analysis of the TDHF wave function using the PNP method and its coupling with statistical-model calculations. For details of the TDHF theory and its application to nuclear systems, see, e.g., Refs. [41–45], and references therein.

A. Cross sections for primary products

Let A_μ, Z_μ, and N_μ, respectively, be mass, charge, and neutron numbers of a projectile ($\mu = \mathrm{P}$) and a target ($\mu = \mathrm{T}$). The total numbers of neutrons and protons in the system are $N^{(n)} = N_\mathrm{P} + N_\mathrm{T}$ and $N^{(p)} = Z_\mathrm{P} + Z_\mathrm{T}$, respectively. The total number of nucleons is denoted as $A = N^{(n)} + N^{(p)}$.

Suppose that we have performed a TDHF calculation for a reaction at a given energy E and an impact parameter b, and we observed generation of binary reaction products. Now we have a many-body wave function at a certain time $t = t_\mathrm{f}$ after collision, which is given by a single Slater determinant:

$$\Psi(\boldsymbol{r}_1\sigma_1 q_1,\ldots,\boldsymbol{r}_A\sigma_A q_A,t_\mathrm{f}) = \frac{1}{\sqrt{A!}}\det\left\{\psi_i^{(q_j)}(\boldsymbol{r}_j\sigma_j,t_\mathrm{f})\right\}, \quad (1)$$

where $\psi_i^{(q)}(\boldsymbol{r}\sigma,t_\mathrm{f})$ is ith single-particle orbital at $t = t_\mathrm{f}$ with spatial, spin, and isospin coordinates $\boldsymbol{r}$, σ, and q, respectively. Our aim is to evaluate production cross sections for *secondary* reaction products based on the TDHF wave function after collision, Eq. (1).

Because of possible nucleon transfer processes, the TDHF wave function after collision is, in general, not an eigenstate of a number operator in a subspace V that contains one of the reaction products, but a superposition of states with different particle-number distributions:

$$|\Psi\rangle = \sum_{N,Z}|\Psi_{N,Z}\rangle, \quad (2)$$

where N and Z specify neutron and proton numbers of a reaction product inside the spatial region V, respectively. Here and henceforth, brackets, such as $|\Psi\rangle$ and $|\psi_i^{(q)}\rangle$, are often used omitting indexes to simplify notations. $|\Psi_{N,Z}\rangle$ can be expressed as

$$|\Psi_{N,Z}\rangle = \hat{P}_N^{(n)}\hat{P}_Z^{(p)}|\Psi\rangle, \quad (3)$$

where $\hat{P}_n^{(q)}$ is the PNP operator for neutrons ($q = n$) or protons ($q = p$),

$$\hat{P}_n^{(q)} = \frac{1}{2\pi}\int_0^{2\pi} e^{i(n-\hat{N}_V^{(q)})\theta}d\theta. \quad (4)$$

$\hat{N}_V^{(q)}$ is the number operator for neutrons ($q = n$) or protons ($q = p$) in the spatial region V,

$$\hat{N}_V^{(q)} = \int_V\sum_{i=1}^{N^{(q)}}\delta(\boldsymbol{r}-\hat{\boldsymbol{r}}_i)\,d\boldsymbol{r} = \sum_{i=1}^{N^{(q)}}\Theta_V(\hat{\boldsymbol{r}}_i), \quad (5)$$

where

$$\Theta_V(\boldsymbol{r}) = \begin{cases} 1 & \text{for } \boldsymbol{r} \in V, \\ 0 & \text{for } \boldsymbol{r} \notin V. \end{cases} \tag{6}$$

The probability that a reaction product composed of N neutrons and Z protons is produced, $P_{N,Z}$, is given by

$$P_{N,Z} = \langle \Psi_{N,Z} | \Psi_{N,Z} \rangle = P_N^{(n)} P_Z^{(p)}. \tag{7}$$

Note that $P_{N,Z}$ is a product of probabilities for neutrons $P_N^{(n)}$ and for protons $P_Z^{(p)}$ in TDHF. These probabilities can be expressed in terms of the single-particle orbitals as

$$P_n^{(q)} = \frac{1}{2\pi} \int_0^{2\pi} e^{in\theta} \det \mathcal{B}^{(q)}(\theta)\, d\theta, \tag{8}$$

where

$$\begin{aligned} (\mathcal{B}^{(q)}(\theta))_{ij} &= \sum_\sigma \int \psi_i^{(q)*}(\boldsymbol{r}\sigma) \psi_j^{(q)}(\boldsymbol{r}\sigma,\theta)\, d\boldsymbol{r} \\ &\equiv \langle \psi_i^{(q)} | \psi_j^{(q)}(\theta) \rangle, \end{aligned} \tag{9}$$

with

$$\psi_i^{(q)}(\boldsymbol{r}\sigma,\theta) = [\Theta_{\bar{V}}(\mathbf{r}) + e^{-i\theta}\Theta_V(\mathbf{r})]\psi_i^{(q)}(\boldsymbol{r}\sigma). \tag{10}$$

By repeating TDHF calculations for various impact parameters b at a given incident energy E, we obtain $P_{N,Z}(b,E)$. The production cross section for a *primary* reaction product composed of N neutrons and Z protons before secondary deexcitation is then given by

$$\sigma_{N,Z}(E) = 2\pi \int_{b_{\min}}^{b_{\rm cut}} b\, P_{N,Z}(b,E)\, db, \tag{11}$$

where $b_{\min}$ is the minimum impact parameter for binary reactions, inside which fusion reactions take place; $b_{\rm cut}$ is a cutoff impact parameter for the numerical integration. Note that if $b_{\rm cut}$ is chosen large enough it merely affects magnitude of the cross section for the elastic scattering.

B. Total angular momentum

In Ref. [47], the PNP method was extended to calculate the expectation value of operators. The method allows one to evaluate the total angular momentum J of a reaction product in each transfer channel, which is an input of a statistical-model calculation.

The idea [47] was to introduce operators for a reaction product inside the spatial region V. In the case of the total angular momentum operator, it can be expressed as

$$\hat{\boldsymbol{J}}_V = \sum_{i=1}^{A} \Theta_V(\hat{\boldsymbol{r}}_i)\, \hat{\boldsymbol{j}}_i, \tag{12}$$

where $\hat{\boldsymbol{j}}_i = (\hat{\boldsymbol{r}}_i - \boldsymbol{R}_{\rm c.m.}) \times \hat{\boldsymbol{p}}_i + \hat{\boldsymbol{s}}_i$. $\boldsymbol{R}_{\rm c.m.}$ is the center-of-mass position of the reaction product, and $\hat{\boldsymbol{p}}_i$ and $\hat{\boldsymbol{s}}_i$ are the momentum and the spin operators, respectively,

The expectation value of the total angular momentum of a reaction product composed of N neutrons and Z protons is then defined as

$$\boldsymbol{J}_{N,Z} = \frac{\langle \Psi_{N,Z} | \hat{\boldsymbol{J}}_V | \Psi_{N,Z} \rangle}{\langle \Psi_{N,Z} | \Psi_{N,Z} \rangle} = \boldsymbol{J}_N^{(n)} + \boldsymbol{J}_Z^{(p)}. \tag{13}$$

It satisfies an identity, $\langle \Psi | \hat{\boldsymbol{J}}_V | \Psi \rangle = \sum_{N,Z} P_{N,Z} \boldsymbol{J}_{N,Z}$. The contribution from neutrons ($q = n$) or protons ($q = p$) is given by

$$\boldsymbol{J}_n^{(q)} = \frac{1}{2\pi P_n^{(q)}} \int_0^{2\pi} e^{in\theta} \det \mathcal{B}^{(q)}(\theta) \sum_{i=1}^{N^{(q)}} \langle \psi_i^{(q)} | \hat{\boldsymbol{j}} | \tilde{\psi}_i^{(q)}(\theta) \rangle_V d\theta, \tag{14}$$

where

$$\tilde{\psi}_i^{(q)}(\boldsymbol{r}\sigma,\theta) \equiv \sum_{j=1}^{N^{(q)}} \psi_j^{(q)}(\boldsymbol{r}\sigma,\theta)(\mathcal{B}^{(q)}(\theta))^{-1}_{ji}. \tag{15}$$

Note that $\{\tilde{\psi}_i(\theta)\}$ are biorthonormal to $\{\psi_i\}$, i.e., $\langle \psi_i | \tilde{\psi}_j(\theta) \rangle = \delta_{ij}$. The subscript V of the bracket in Eq. (14) indicates that the spatial integration is taken only over the spatial region V. In practice, the total angular momentum perpendicular to the reaction plane will be used as an input for statistical-model calculations. It will be denoted simply as $J_{N,Z}$.

C. Excitation energy

Applying the PNP method, we can also evaluate the excitation energy E^* of a reaction product in each transfer channel [47]. The energy expectation value of a reaction product composed of N neutrons and Z protons is defined as

$$E_{N,Z} = \frac{\langle \Psi_{N,Z} | \hat{H}_V | \Psi_{N,Z} \rangle}{\langle \Psi_{N,Z} | \Psi_{N,Z} \rangle}, \tag{16}$$

where $\hat{H}_V$ is a Hamiltonian for a reaction product inside the spatial region V. There also follows an identity, $\langle \Psi | \hat{H}_V | \Psi \rangle = \sum_{N,Z} P_{N,Z} E_{N,Z}$.

In practice, one may work with an energy density functional (EDF). In such a case, $E_{N,Z}$ is given by

$$\begin{aligned} E_{N,Z} = \frac{1}{4\pi^2 P_N^{(n)} P_Z^{(p)}} &\int_0^{2\pi} \int_0^{2\pi} e^{i(N\theta + Z\varphi)} \\ &\times \det \mathcal{B}(\theta,\varphi) \int_V \mathcal{E}(\boldsymbol{r},\theta,\varphi)\, d\boldsymbol{r}\, d\theta\, d\varphi, \end{aligned} \tag{17}$$

where $\det \mathcal{B}(\theta,\varphi) = \det \mathcal{B}^{(n)}(\theta) \det \mathcal{B}^{(p)}(\varphi)$. $\mathcal{E}(\boldsymbol{r},\theta,\varphi)$ denotes an EDF kernel which has the same form as the EDF used, but is composed of complex mixed densities, e.g., $\rho_q(\boldsymbol{r},\theta) = \sum_{i,\sigma} \psi_i^{(q)*}(\boldsymbol{r}\sigma)\tilde{\psi}_i^{(q)}(\boldsymbol{r}\sigma,\theta)$, etc.

For our purpose, Eq. (16) or Eq. (17) should be evaluated in the rest frame of the reaction product to remove kinetic energy associated with center-of-mass translational motion. Regarding it as internal energy of the reaction product, excitation energy can be evaluated as

$$E^*_{N,Z} = E_{N,Z} - E^{\rm g.s.}_{N,Z}, \tag{18}$$

where $E^{\rm g.s.}_{N,Z}$ denotes energy of a nucleus specified by N neutrons and Z protons in its Hartree-Fock ground state.

D. Cross sections for secondary products

Having $P_{N,Z}$, $J_{N,Z}$, and $E^*_{N,Z}$ at hand, we can apply a statistical model to obtain production cross sections for *secondary* reaction products. In this paper, GEMINI++ [53] is employed. For a given set of (N, Z, E^*, J), GEMINI++ provides a sequence of statistically selected binary decays, including both particle evaporation and fission, until it becomes energetically forbidden or improbable because of competing γ-ray emission.

Because of its statistical nature, a different sequence of binary decays can be obtained with the same set of (N, Z, E^*, J). To evaluate decay probabilities, one may repeat computations of a binary-decay sequence, let's say, $N_{\rm trial}$ times. Among the obtained $N_{\rm trial}$ decay sequences, one can count the number of processes in which a sequence of deexcitation processes of a primary reaction product composed of N neutrons and Z protons ends up with a nucleus specified by N' neutrons and Z' protons. Then, denoting it as $N_{N',Z'}$, the decay probability for the process $(N,Z) \rightarrow (N',Z')$ can be defined by

$$P_{\rm decay}(E^*_{N,Z}, J_{N,Z}, N, Z; N', Z') = \frac{N_{N',Z'}}{N_{\rm trial}}. \tag{19}$$

The number $N_{\rm trial}$ sets a lower limit on the decay probabilities, because processes with $P_{\rm decay} \lesssim 1/N_{\rm trial}$ will not be taken into account.

The cross section for a *secondary* reaction product after evaporation and/or fission processes is then evaluated as

$$\tilde{\sigma}_{N',Z'}(E) = 2\pi \int_{b_{\rm min}}^{b_{\rm cut}} b\, \widetilde{P}_{N',Z'}(b,E)\, db, \tag{20}$$

where $\widetilde{P}_{N',Z'}$ denotes the probability that a reaction product composed of N' neutrons and Z' protons is produced after secondary deexcitation processes:

$$\widetilde{P}_{N',Z'} = \sum_{N \geqslant N'} \sum_{Z \geqslant Z'} P_{N,Z}\, P_{\rm decay}(E^*_{N,Z}, J_{N,Z}, N, Z; N', Z'). \tag{21}$$

Note that the input quantities, $P_{N,Z}$, $J_{N,Z}$, and $E^*_{N,Z}$, are dependent on the incident energy E and the impact parameter b.

E. Computational details

For the TDHF calculation and the PNP analysis, our own computational code was extended and applied [48]. In the code, single-particle orbitals are represented on three-dimensional Cartesian coordinates (without any symmetry restrictions) with isolated boundary conditions. The lattice spacing is set to 0.8 fm. Spatial derivatives are computed with the 11-point finite-difference formula. For time evolution, the fourth-order Taylor expansion method is used with a single predictor-corrector step. The time step is set to $0.2\,{\rm fm}/c$. The Coulomb potential is computed using Fourier transformations. For the EDF, the Skyrme SLy5 functional [67] is employed.

Note that results of the PNP analysis with Eqs. (7), (13), and (16) are invariant under unitary transformations for the single-particle orbitals, $\psi'_i(\boldsymbol{r}\sigma) = \sum_j \mathcal{U}_{ij}\psi_j(\boldsymbol{r}\sigma)$, where $\mathcal{U}$ is a unitary matrix: It only changes the phase of the many-body wave function, i.e., $\Psi' = \det\mathcal{U}\,\Psi$. Thus, the quantities are well defined and the results may merely depend on the accuracy of the numerical integration and the choice of the spatial region V. The latter is expected to be small in the case where reaction products are well separated spatially. In the present analysis, V is taken as a sphere with a radius R_V around the center of mass of a reaction product. Indeed, it was confirmed, by varying R_V from 11 to 15 fm for the ^{40}Ca + ^{124}Sn system, that $J_{N,Z}$ and $E_{N,Z}$ of lighter fragments are affected only less than $0.01\,\hbar$ and a few tens of keV, respectively.

The numerical integration over the gauge angle $[0,2\pi]$ is performed using the trapezoidal rule with an M-point uniform mesh. $P_{N,Z}$ and $J_{N,Z}$ can be stably computed for all transfer channels and do not depend on M, if it is taken larger than $M \approx$ 100–200 for the systems analyzed in the present paper. The accuracy of $E_{N,Z}$, on the other hand, is somewhat worse, which depends on the probability $P_{N,Z}$. For example, for different values of M (200–500), $E_{N,Z}$ varies roughly several keV for a main process with $P_{N,Z} \approx 10^{-1}$, whereas for a process with smaller probabilities, $P_{N,Z} \approx 10^{-5}$, the difference can be several hundreds of keV. Moreover, the absolute value of $E_{N,Z}$ becomes unphysically large for processes with tiny probabilities, $P_{N,Z} \lesssim 10^{-5}$, as was observed for a lighter system [47]. In the present paper, $M = 300$ and $R_V = 15\,{\rm fm}$ are utilized. It ensures at least 1-MeV accuracy of $E_{N,Z}$, which would be sufficient for the present purpose of quantifying effects of secondary deexcitation processes on production cross sections.

The ground-state energy of nuclei, $E^{\rm g.s.}_{N,Z}$ in Eq. (18), is computed employing a cubic box with 20.8 fm on each side. The mesh spacing is set to 0.8 fm, as in the TDHF calculations. To find the energy minimum solution, avoiding those in local minima, static Hartree-Fock calculations are first performed with constraints on various deformation parameters ($\beta = 0$, and $\beta = 0.1, 0.2$ with $\gamma = 0^\circ, 30^\circ, 60^\circ$). After getting a moderately convergent solution, the constraints on β and γ are released, and the energy is re-minimized. The state with the lowest energy among the seven candidates is regarded as the Hartree-Fock ground state. The ground-state energies of various isotopes with $Z \leqslant 35$ are prepared for the evaluation of excitation energies of respective transfer products. Equal-filling treatment is adopted for an odd number of nucleons, where the last nucleon resides in a time-reversal pair of orbitals with half occupation.

To describe secondary processes, the statistical compound-nucleus deexcitation model, GEMINI++ [53], is employed. GEMINI++ is an improved version of a statistical model, GEMINI, developed by Charity [68]. It takes into account not only evaporation of light particles, i.e., n, p, d, t, ^{3}He, α, ^{6}He, $^{6-8}$Li, and $^{7-10}$Be, with the Hauser-Feshbach formalism [69], but also emission of heavier fragments with a binary-decay formalism of Moretto [70], as well as fission based on the Bohr-Wheeler formalism [71]. The default setting of the code is used for all reactions analyzed in the present paper. The ingredients of the statistical model have been parametrized and determined so as to allow a good systematic description of the evaporation spectra for the entire mass region. Detailed discussions on various modifications and fine-tuning of the model parameters that were implemented in the GEMINI++ code can be found in Refs. [72,73]. It was

TABLE I. A list of information of the reactions investigated.

System	$E_{\mathrm{c.m.}}$ (MeV)	N_P/Z_P	N_T/Z_T	Z_PZ_T	Expt.
^{40}Ca + ^{124}Sn	128.54	1.00	1.48	1000	[74]
^{48}Ca + ^{124}Sn	125.44	1.40	1.48	1000	[75]
^{40}Ca + ^{208}Pb	208.84	1.00	1.54	1640	[76]
^{58}Ni + ^{208}Pb	256.79	1.07	1.54	2296	[77]
^{64}Ni + ^{238}U	307.35	1.29	1.57	2576	[78]
^{136}Xe + ^{198}Pt	644.98	1.52	1.54	4212	[79]

tested, for all the systems under study (see Table I), that $N_{\mathrm{trial}} = 100$, 1000, and 10 000 provide almost identical cross sections. (Even $N_{\mathrm{trial}} = 10$ gives very similar cross sections, because of neutron evaporation dominance in those reactions.) In the following, results obtained with $N_{\mathrm{trial}} = 1000$ are presented.

III. RESULTS AND DISCUSSION

In the present paper, TDHF+GEMINI is applied to six reaction systems listed in Table I, for which precise experimental data are available. One should note that the reactions investigated cover a range of systems which are expected to show different properties of the reaction dynamics. In reactions of projectile and target nuclei with different N/Z ratios, the charge equilibration process takes place [80], where neutrons and protons are transferred toward the opposite directions, to reduce the N/Z imbalance of the colliding nuclei. Fusion reaction in a system with a large charge product exceeding a critical value, $Z_PZ_T \gtrsim 1600$, is known to be substantially hindered [81]. Those characteristic quantities are also listed in Table I.

A detailed analysis of the TDHF results for MNT processes in the ^{40,48}Ca + ^{124}Sn, ^{40}Ca + ^{208}Pb, and ^{58}Ni + ^{208}Pb reactions was carried out in Ref. [46]. Recently, TDHF calculations for MNT and QF processes in the ^{64}Ni + ^{238}U reaction were also performed. Comprehensive discussions on interplay between orientations of deformed ^{238}U and quantum shells in the reaction dynamics can be found in Ref. [50]. Here, the same TDHF wave functions are re-analyzed applying TDHF+GEMINI.

TDHF calculations for the ^{136}Xe + ^{198}Pt reaction have been newly performed. The ground state of ^{136}Xe and ^{198}Pt turned out to be slightly deformed in a triaxial shape with deformation parameters, ($\beta \simeq 0.06$, $\gamma \simeq 29^\circ$) and ($\beta \simeq 0.12$, $\gamma \simeq 33^\circ$), respectively. Those nuclei were placed in such a way that the axis around which $|Q_{22}|$ takes the smallest value is set perpendicular to the reaction plane. TDHF calculations were performed for various impact parameters in a range of [0, 12] (fm). No fusion reaction was observed for all impact parameters. Reaction mechanisms including incident energy dependence will be investigated in the forthcoming paper. In this paper, we will focus on the production cross sections for the $E_{\mathrm{c.m.}} \simeq 644.98$ MeV case.

It would be useful to first digest success and failure of the TDHF description. Because of the microscopic nature of the TDHF theory, it was not known, before our study

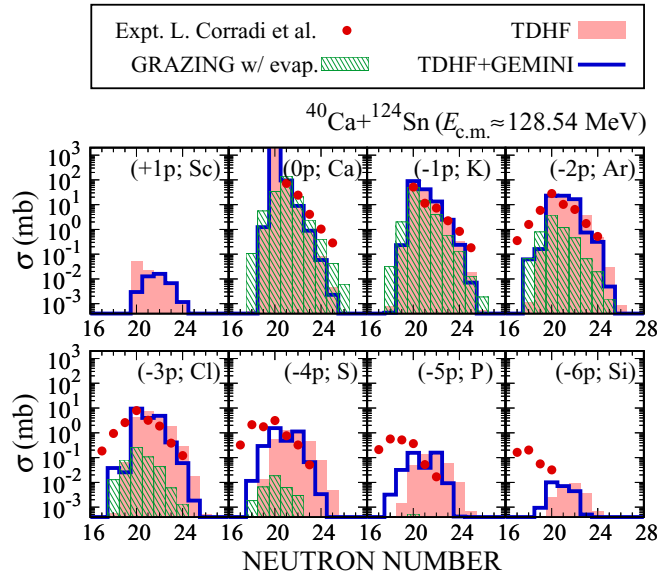

FIG. 1. Production cross sections for lighter fragments in the ^{40}Ca + ^{124}Sn reaction at $E_{\mathrm{c.m.}} \simeq 128.54$ MeV. Each panel shows cross sections for different proton-transfer channels. The horizontal axis is the neutron number of the fragments. Red filled circles denote the experimental data [74]. Red filled areas represent TDHF results for primary reaction products. Cross sections for secondary reaction products obtained with TDHF+GEMINI are shown by blue solid lines. For comparison, GRAZING results [82] are also shown by green shaded histograms.

[46], to what extent TDHF can quantitatively describe cross sections for MNT processes. By performing a number of TDHF calculations for various impact parameters b and by plugging $P_{N,Z}(b)$ into Eq. (11), one can evaluate production cross sections for primary reaction products, based on the TDHF calculations. It should be noted here that no empirical parameters are introduced that can be adjusted to reproduce experimental data.

The calculations were first performed for the ^{40,48}Ca + ^{124}Sn, ^{40}Ca + ^{208}Pb, and ^{58}Ni + ^{208}Pb reactions [46]. In Figs. 1–4, production cross sections for lighter (projectilelike) fragments are shown. Cross sections are classified according to the number of transferred protons x, indicated by ($\pm x$p; X),

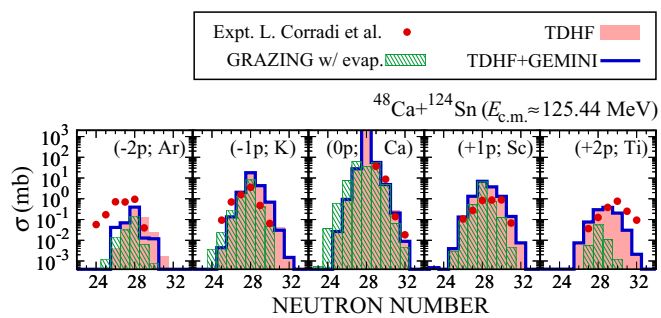

FIG. 2. Same as Fig. 1, but for the ^{48}Ca + ^{124}Sn reaction at $E_{\mathrm{c.m.}} \simeq 125.44$ MeV. The experimental data were reported in Ref. [75].

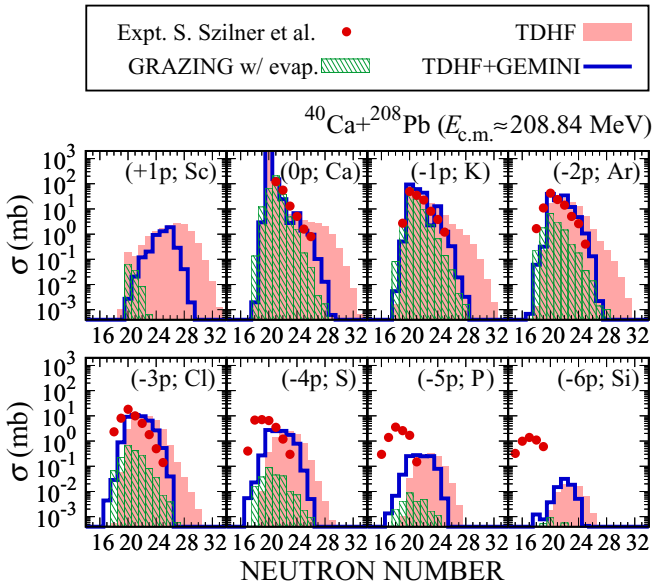

FIG. 3. Same as Figs. 1 and 2, but for the ^{40}Ca + ^{208}Pb reaction at $E_{c.m.} \simeq 208.84$ MeV. The data for $E_{c.m.} \simeq 197.10$ MeV were also analyzed, getting very similar results (not shown). The experimental data were reported in Ref. [76].

where X stands for the corresponding element. The plus sign corresponds to proton transfer from the target to the projectile (pickup), while the minus sign corresponds to the opposite (stripping). The horizontal axis is the neutron number of the fragments. Experimental data are shown by red filled circles. The cross sections for *primary* reaction products obtained from the TDHF calculations [46] are shown by red filled areas.

It is evident from the figures that TDHF nicely captures the main features of the reaction dynamics. In the reactions

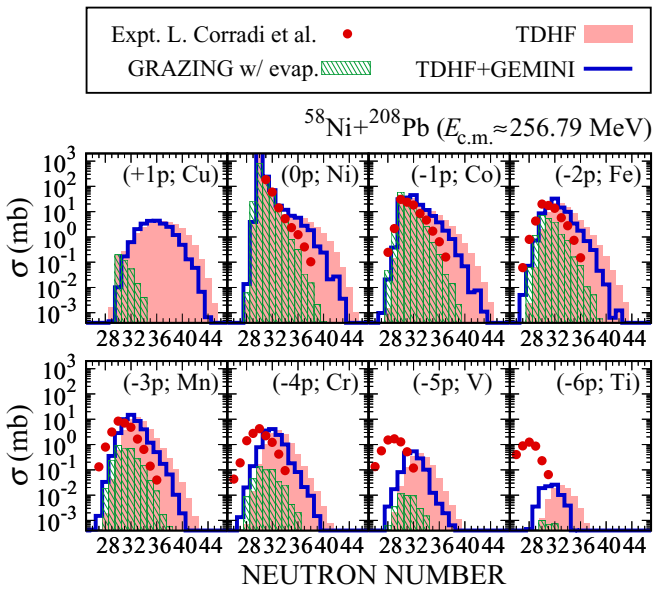

FIG. 4. Same as Figs. 1–3, but for the ^{58}Ni + ^{208}Pb reaction at $E_{c.m.} \simeq 256.79$ MeV. The experimental data were reported in Ref. [77].

with a large N/Z asymmetry (^{40}Ca + ^{124}Sn, ^{40}Ca + ^{208}Pb, and ^{58}Ni + ^{208}Pb), neutron pickup and proton stripping are favored, because of the charge equilibration process (Figs. 1, 3, and 4). On the other hand, in the ^{48}Ca + ^{124}Sn reaction where N/Z ratios of the projectile and the target are already very close to each other, the number of transferred nucleons becomes very small on average, resulting in the transfer of neutrons and protons in both directions (Fig. 2).

From a careful look at the figures, one can see that TDHF quantitatively reproduces the measured cross sections for few-nucleon transfer processes: e.g., processes with pickup of a few neutrons in $(0p)$, $(\pm 1p)$, and $(-2p)$ proton-transfer channels. The agreements are noteworthy, because no adjustable parameters are included in the calculations. However, there exist discrepancies between the TDHF results and the experimental data. Namely, the measurements show that substantial cross sections for fragments with a smaller number of neutrons emerge when more than one protons are transferred. TDHF fails to reproduce the observed tendency. Moreover, cross sections for multiproton stripping processes are considerably underestimated by the TDHF calculations. On the other hand, in the ^{40}Ca + ^{208}Pb and ^{58}Ni + ^{208}Pb reactions, TDHF overestimates cross sections for pickup of many neutrons in $(0p)$, $(-1p)$, and $(-2p)$ channels. The latter originated from trajectories at small impact parameters accompanying large energy losses, where dynamics of a thick-neck formation and its breaking is responsible for the amount of nucleon transfer (see Ref. [46] for a detailed discussion).

One can expect that the discrepancies may be remedied by including secondary deexcitation processes in the TDHF description. After transfer of many nucleons reaction products can be highly excited, and what were measured experimentally must be the cross sections for secondary products after deexcitation processes. For example, if neutrons were evaporated from primary reaction products, the resulting cross sections would shift toward less neutron-number side, the left direction in the figures; if protons were emitted to the continuum, then the cross sections would be redistributed to channels classified as a process with a larger number of stripping of protons. It is now feasible to disentangle the possible origins of the discrepancies owing to TDHF+GEMINI.

In Figs. 1–4, the cross sections for *secondary* reaction products obtained with TDHF+GEMINI are represented by blue solid lines. In the evaluation of the cross sections, the PNP calculations for $J_{N,Z}$ and $E^*_{N,Z}$ presented in Secs. II B and II C, respectively, were fully performed for all impact parameters investigated. For comparison, online GRAZING calculations [82] which include neutron-evaporation effects were also performed, and the results are shown by green shaded histograms.

From the figures, one can see that the inclusion of secondary deexcitation processes improves the description. For instance, TDHF+GEMINI quantitatively reproduces the experimental data, mainly for neutron-pickup processes, accompanying stripping of several protons. The description of the overestimated cross sections of neutron-pickup processes for $(0p)$, $(-1p)$, and $(-2p)$ channels in the ^{40}Ca + ^{208}Pb and ^{58}Ni + ^{208}Pb reactions is also improved. However, the effects of secondary deexcitation processes are not large enough to remedy all the discrepancies between the TDHF results and

the experimental data. The peak positions of the cross sections still locate at the larger neutron-number side compared to the experimental data. Note that the magnitude of evaporation effects is very similar to the one observed in the GRAZING calculations as well as our prior attempts [83,84] with a simple evaporation model developed by Dostrovsky *et al.* [85].

It is worth emphasizing here that, although the peak positions are different compared to the experimental cross sections, the absolute value is well reproduced by TDHF+GEMINI up to around the $(-4p)$ channel. The widely used GRAZING calculations provide few orders of magnitude smaller cross sections, when more than one protons are transferred. In Refs. [76,77], the ^{40}Ca + ^{208}Pb and ^{58}Ni + ^{208}Pb reactions were analyzed by the CWKB semiclassical model. It provides quantitatively very similar results as the GRAZING calculations, i.e., the absolute values of the cross sections for $(-xp)$ $(x \geqslant 2)$ channels were substantially underestimated. The authors of Refs. [76,77] phenomenologically introduced pair-transfer modes to explain the experimental data. Although they could obtain better description of the cross sections by adjusting an additional macroscopic form factor to reproduce the experimental cross section for the pure two-proton stripping process without neutron transfer, i.e., the $(0n,-2p)$ channel, the validity of the hypothetical pair-transfer modes was unclear. The present results indicate that the pair-transfer processes may play a minor role, at least for the above-barrier MNT processes, as the absolute value of the cross sections for the $(-2p)$ channel is well reproduced without pairing by TDHF+GEMINI.

The remained discrepancies between the results of TDHF+GEMINI and the experimental data would suggest a limit of the theoretical framework. For example, although we could obtain cross sections for various transfer channels using the PNP method, they merely come from distribution around the average trajectory described by a single Slater determinant. Because of this fact, the peak positions are strongly correlated with the average number of transferred nucleons. Because we do not have a mean-field potential for, e.g., the $(-6p)$ channel, the underestimation of multiproton stripping processes may be an artifact of the usage of the single mean-field potential. In reality, the potential should be transfer-channel dependent. When many protons are removed from the projectile, for instance, the potential felt by neutrons inside the proton-removed (proton-added) nucleus would become shallower (deeper) that may suppress (enhance) neutron pickup (stripping) processes. This transfer-channel dependent potential may explain the observed discrepancies. Part of the effects may be seen as beyond-mean-field fluctuations and correlations. One should note, however, that possible underestimation of evaporation effects has not been excluded yet. For instance, $E^*_{N,Z}$ and $J_{N,Z}$ that were used for the statistical-model calculations are the expectation values of energy and angular momentum of a reaction product in each transfer channel and, thus, are averaged over all possible quantal states populated by the reaction. However, these quantities should have certain distributions, and a substantial part of evaporation processes might originate from components which are not in the vicinity of the mean values. Those distributions may not adequately be described within the TDHF theory, because for evaluation of the variance of them proper description of two- and four-body observables is necessary. In addition, e.g., the neglected prompt (pre-equilibrium) nucleon emissions before compound-nucleus formation and any underestimation of negative Q-value effect would enhance the particle evaporation. In any case, the present results by TDHF+GEMINI suggest that, to fully reproduce experimental cross sections for MNT processes, one should extend the theoretical framework that goes beyond the TDHF theory: e.g., a variational method of Balian and Vénéroni [54,58], stochastic mean-field theory (SMF) [86,87], time-dependent density matrix theory (TDDM) [88–91], time-dependent generator coordinate method (TDGCM) [92,93], multiconfiguration TDHF (MCTDHF) [94,95], and so forth.

It should be emphasized here that, although there still remain certain discrepancies as discussed above, TDHF+GEMINI will be a powerful tool, especially for systems for which no experimental data exist, to figure out optimal conditions to produce objective neutron-rich isotopes, as a microscopic model without empirical parameters that has better accuracy than the widely used semiclassical models. In the following, let us thus consider further applications of TDHF+GEMINI.

Although it is possible to perform the PNP calculations for $J_{N,Z}$ and $E^*_{N,Z}$ as shown above, it requires quite large computational effort. For reactions involving heavy nuclei, for instance, the number of discreet points for the numerical integration over the gauge angles θ and φ is typically a few hundred. Then, to evaluate Eqs. (14) and (17), one needs to compute derivatives of 3D complex spatial functions many times, which could be as time-consuming as a TDHF calculation. Moreover, to compute the excitation energies with Eq. (18), one has to compute the energy of nuclei in their Hartree-Fock ground state in a wide mass region. It would also be problematic if one wants to change the working EDF, then the ground-state energies have to be re-computed for the evaluation of $E^*_{N,Z}$. One may consider using experimental masses for ground-state energies, $E^{\mathrm{g.s.}}_{N,Z}$, however, then the result would be dependent on quality of the EDF itself.

Because it is not desirable to pay much effort for the computation of the input parameters of the statistical-model calculations, let us consider a simpler evaluation. Namely, one may replace $E^*_{N,Z}$ and $J_{N,Z}$ in Eq. (19) with average quantities that can be easily obtained from the TDHF wave function after collision. At the time $t = t_{\mathrm{f}}$ after collision, one can compute the average total angular momentum as

$$\bar{J} = \langle \Psi | \hat{J}_V | \Psi \rangle = \sum_{i=1}^{A} \langle \psi_i | \hat{j} | \psi_i \rangle_V , \tag{22}$$

where operators $\hat{J}_V$ and $\hat{j}$ are those for the component perpendicular to the reaction plane. One can also compute such quantities as average mass and charge numbers, A_i and Z_i $(i = 1,2)$, the relative vector connecting the center-of-mass positions of the reaction products $\boldsymbol{R}$, and its time derivative $\dot{\boldsymbol{R}}$. Then, the average total kinetic energy (TKE) of the outgoing fragments reads

$$\mathrm{TKE} = \frac{1}{2}\mu \dot{\boldsymbol{R}}^2 + \frac{Z_1 Z_2 e^2}{|\boldsymbol{R}|}, \tag{23}$$

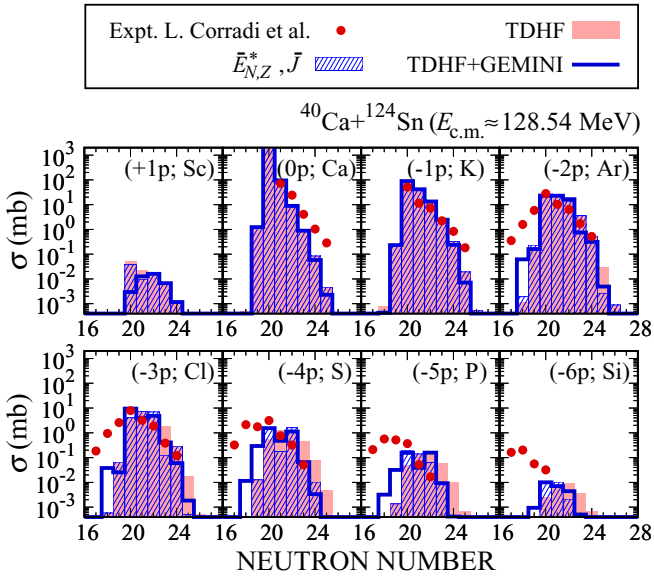

FIG. 5. Same as Fig. 1 for the ^{40}Ca + ^{124}Sn reaction at $E_{\rm c.m.} \simeq$ 128.54 MeV, but cross sections by TDHF+GEMINI with a simpler treatment of E^* and J (see text for details) are shown by blue shaded histograms, instead of GRAZING results.

where $\mu = m_n A_1 A_2/(A_1 + A_2)$ is the reduced mass, m_n being the nucleon mass. From this quantity, average total excitation energy shared by the two fragments may be evaluated as

$$\bar{E}^*_{\rm tot} = E - {\rm TKE} - Q, \tag{24}$$

where E is the incident relative energy and Q denotes the Q value of the reaction. By putting the actual Q value for each transfer channel, $E^*_{\rm tot}$ becomes effectively transfer-channel dependent. To evaluate the Q value for each transfer channel, experimental masses from the latest atomic mass evaluation, AME2016 [96,97], are utilized, whenever available; for nuclei whose mass has not been measured experimentally, theoretical values from the newest version of the finite-range droplet model, FRDM(2012) [98], are adopted. One may distribute the total excitation energy to respective reaction products in such a way that it is proportional to their mass:

$$\bar{E}^*_{N,Z} = \frac{N+Z}{A_1+A_2}\,\bar{E}^*_{\rm tot}. \tag{25}$$

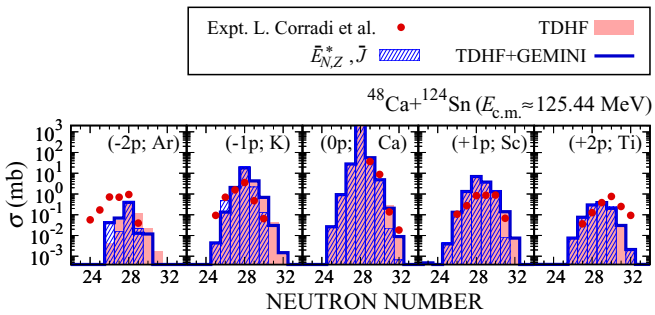

FIG. 6. Same as Fig. 5, but for the ^{48}Ca + ^{124}Sn reaction at $E_{\rm c.m.} \simeq$ 125.44 MeV.

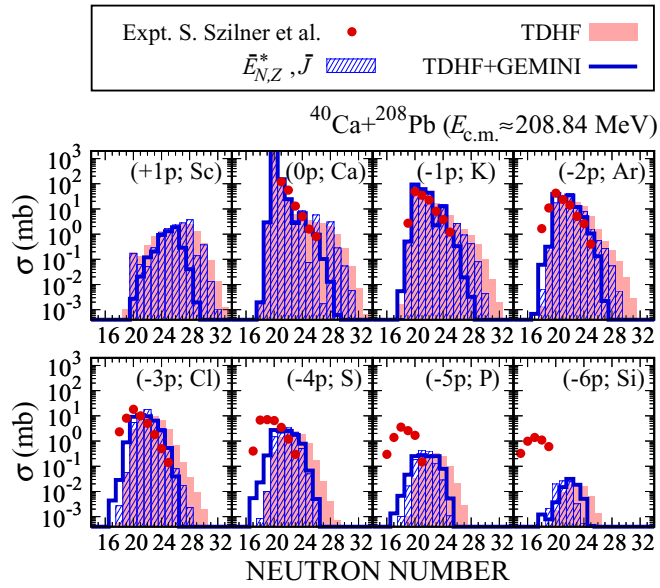

FIG. 7. Same as Figs. 5 and 6, but for the ^{40}Ca + ^{208}Pb reaction at $E_{\rm c.m.} \simeq$ 208.84 MeV.

It is equivalent to assume that the thermal equilibrium is realized before formation of the fragments. The assumption may not always be correct especially in a transitional regime from quasielastic to deep-inelastic reactions. However, because in such a regime energy loss is not that large and secondary processes play a less important role, genuineness of the assumption may not be significant.

The results of TDHF+GEMINI calculations with the average quantities, $\bar{E}^*_{N,Z}$ and $\bar{J}$, are presented in Figs. 5–8 by blue shaded histograms. As seen in the figures, this treatment provides quantitatively similar results as those obtained with the elaborated PNP calculations (blue solid lines, same as Figs. 1–4). For some channels, evaporation effects are less pronounced (e.g., for the ^{40}Ca + ^{124}Sn reaction shown in Fig. 5), which might be from the assumption that the excitation energy is shared as it is proportional to fragment masses. On the other hand, the angular momentum effects on neutron evaporation processes turned out to be negligibly small in the reactions investigated. It may play a certain role in fission processes of heavier fragments, and the validity of using $\bar{J}$ should be re-examined for such cases. Nevertheless, the results shown in Figs. 1–8 may support the usage of the average values for the evaluation of secondary deexcitation processes, significantly reducing the computational cost. In the following, TDHF+GEMINI is applied to the ^{64}Ni + ^{238}U and ^{136}Xe + ^{198}Pt reactions employing the simpler treatment with the average values, $\bar{E}^*_{N,Z}$ and $\bar{J}$, for statistical-model calculations [we will keep the usage of Eq. (25) as a simple, conservative choice].

Figure 9 shows production cross sections for the ^{64}Ni + ^{238}U reaction at $E_{\rm c.m.} \simeq$ 307.35 MeV. Although ^{238}U is largely deformed in a prolate shape, it was shown that MNT processes in peripheral collisions do not depend much on the nuclear orientations [50]. Here, the results of side collisions (z-direction case in Ref. [50]), where the symmetry axis of ^{238}U is always

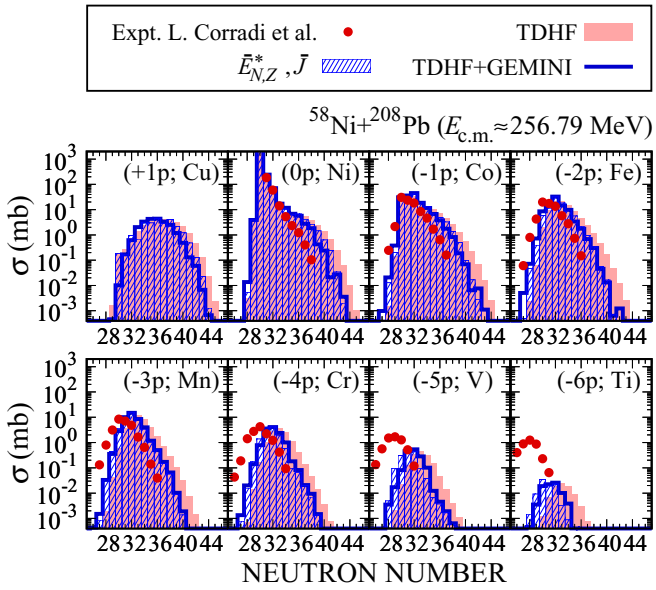

FIG. 8. Same as Figs. 5–7, but for the ^{58}Ni + ^{208}Pb reaction at $E_{\rm c.m.} \simeq 256.79$ MeV.

set perpendicular to the reaction plane, are shown for better visibility. (Other cases resulted in quantitatively similar cross sections.) Because the ^{64}Ni + ^{238}U reaction has a relatively large N/Z asymmetry, neutron-pickup and proton-stripping processes dominate the nucleon transfer. The agreement and disagreement are indeed similar to the ^{40}Ca + ^{124}Sn, ^{40}Ca + ^{208}Pb, and ^{58}Ni + ^{208}Pb cases shown in Figs. 1, 3, and 4 (and Figs. 5, 7, and 8). A characteristic feature specific to the ^{64}Ni + ^{238}U reaction is that cross sections were measured also for proton-pickup processes, $(+1p)$ and $(+2p)$. While GRAZING substantially underestimates those cross sections, especially for the $(+2p)$ channel, TDHF+GEMINI provides significant cross sections, even greater than the experimental data. In TDHF, the latter originated from a transitional regime from quasielastic to more complicated reactions, like deep-inelastic and QF processes. Indeed, if we exclude contributions from small impact parameters ($b \lesssim 4$ fm), where energy loss is already saturated [50], the overestimation of cross sections for proton-pickup processes can be removed, leaving cross sections for proton-stripping processes almost unaffected. Similarly, the "shoulders" from the overestimation of neutron-pickup processes seen in Figs. 3 and 4 (and Figs. 7 and 8) for the ^{40}Ca + ^{208}Pb and ^{58}Ni + ^{208}Pb reactions can be removed if one excludes contributions from small impact parameters, where the onset of the mass equilibration process through a thick-neck formation and its breaking is observed [46]. However, all figures in the present paper show cross sections obtained by integration over the full impact-parameter range, avoiding any *ad hoc* manipulation of the obtained results.

The primary goal of this work is to predict optimal conditions to produce new neutron-rich unstable isotopes. Aiming at production of neutron-rich nuclei around the neutron magic number $N = 126$, whose properties are crucial to understand the detailed scenario of the r-process nucleosynthesis, an experiment was recently carried out for the ^{136}Xe + ^{198}Pt reaction [79]. In Ref. [79], production cross sections for heavier (targetlike) fragments were deduced from detected outcomes with respect to lighter (projectilelike) fragments, obtaining promising results. Thus, the comparison with the experimental data for this system and TDHF+GEMINI is expected to be a benchmark to check the accuracy and usefulness of the proposed method.

In Fig. 10, production cross sections for the ^{136}Xe + ^{198}Pt reaction at $E_{\rm c.m.} \simeq 644.98$ MeV are shown. It should be noted here that the projectile and the target have very similar N/Z ratios (cf. Table I), and one expects transfer of neutrons and protons toward both directions (similar to the ^{48}Ca + ^{124}Sn reaction shown in Figs. 2 and 6). By comparing the cross

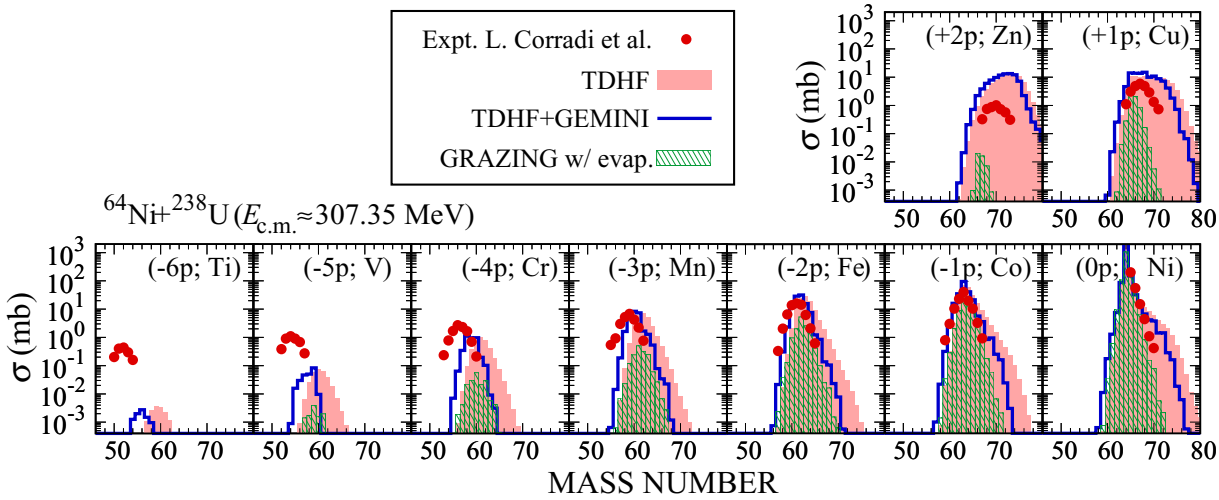

FIG. 9. Production cross sections for lighter fragments in the ^{64}Ni + ^{238}U reaction at $E_{\rm c.m.} \simeq 307.35$ MeV. Each panel shows cross sections for different proton-transfer channels. The horizontal axis is the mass number of the fragments. Cross sections associated with side collisions are shown (see text). Cross sections for secondary products evaluated by TDHF+GEMINI (with $\bar{E}^*_{N,Z}$ and $\bar{J}$ as in Figs. 5–8) are shown by blue solid lines. The experimental data were reported in Ref. [78]. GRAZING results [82] are also shown by green shaded histograms, for comparison.

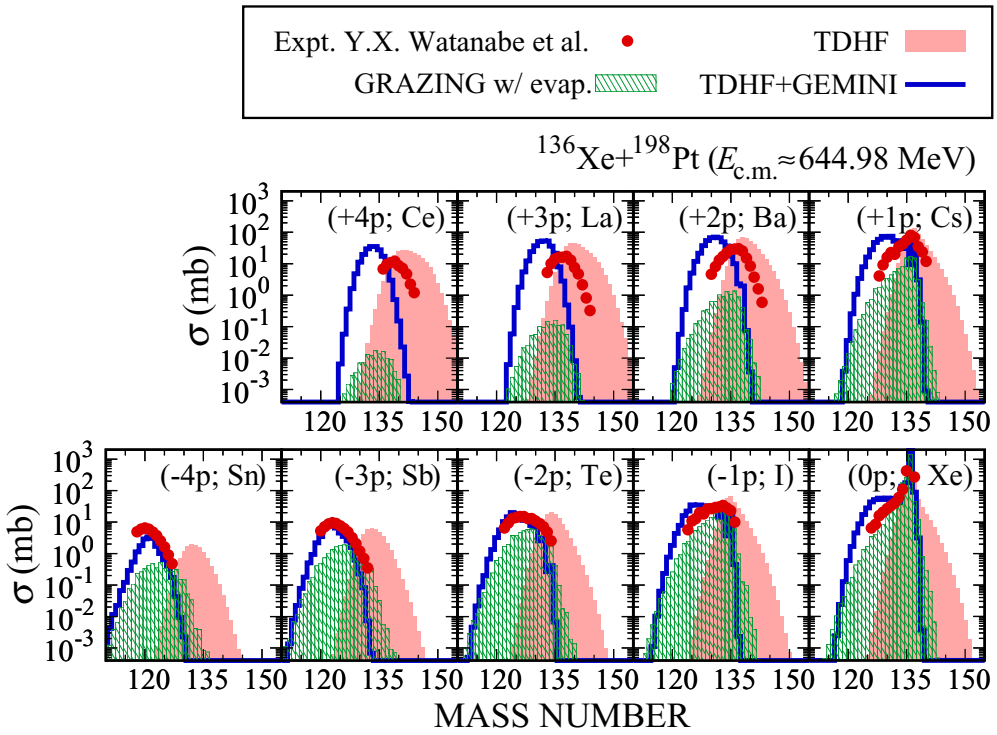

FIG. 10. Same as Fig. 9, but for the ^{136}Xe + ^{198}Pt reaction at $E_{\mathrm{c.m.}} \simeq 644.98$ MeV. The experimental data and the GRAZING results were taken from Ref. [79] (see [99] for a comment on this point).

sections for primary (red filled areas) and secondary (blue solid lines) reaction products, one can see significant effects of deexcitation processes. For proton-stripping channels ($-xp$), TDHF+GEMINI reproduces the measurements surprisingly well, both the magnitude and the centroid of the cross sections for the secondary products. On the other hand, too large deexcitation effects are observed for proton-pickup channels ($+xp$). This type of disagreement is peculiar to the ^{136}Xe + ^{198}Pt reaction. The experimental data indicate that reaction products in proton-pickup channels might be less excited compared to those in proton-stripping channels. Note that GRAZING also provides similar magnitude of evaporation effects, although the absolute value of the cross sections is substantially underestimated.

Lastly, it should be remembered that TDHF+GEMINI also allows one to evaluate production cross sections for heavier fragments, where transfer-induced fission is expected to play an important role. Detailed investigation of production mechanisms of heavy neutron-rich nuclei which survive against transfer-induced fission as well as particle evaporation is the next step of this work.

IV. SUMMARY

In this paper, a method, called TDHF+GEMINI, was proposed, which enables us to evaluate production cross sections for *secondary* products in low-energy heavy ion reactions. In the method, the reaction dynamics, on the time scale of 10^{-21}–10^{-20} s, is described microscopically based on the time-dependent Hartree-Fock (TDHF) theory. Production probabilities, total angular momenta, and excitation energies of primary reaction products are extracted from the TDHF wave function after collision, using the particle-number projection method. Based on those quantities derived from TDHF, secondary deexcitation processes of primary reaction products, including both particle evaporation and fission, are described employing the GEMINI++ compound-nucleus deexcitation model.

The method was applied to ^{40,48}Ca + ^{124}Sn, ^{40}Ca + ^{208}Pb, ^{58}Ni + ^{208}Pb, ^{64}Ni + ^{238}U, and ^{136}Xe + ^{198}Pt reactions for which precisely measured experimental cross sections are available. The inclusion of deexcitation effects, which are dominated by neutron evaporation in the present cases, changes the cross sections toward the direction consistent with the experimental data. However, there still remain discrepancies between the measured cross sections and the TDHF+GEMINI results, especially for multiproton transfer processes. It may indicate the importance of description going beyond the standard self-consistent mean-field theory to correctly describe multinucleon transfer processes in low-energy heavy ion reactions.

In conclusion, it was demonstrated that, even though some discrepancy still remains, the combination of TDHF and a statistical model offers an excellent starting point toward a complete modeling of low-energy heavy ion reactions. It is important to stress that, in the proposed method, there is no room to adjust the model parameters specific to each reaction: Energy density functional is determined so as to reproduce known properties of finite nuclei and nuclear matter [67]; GEMINI++ [53] and its ongoing developments [72,73] allow a systematic reproduction of a large body of data for the entire mass region. Therefore, it will be a promising tool that can

predict, in a nonempirical way, optimal reaction mechanisms to produce new neutron-rich isotopes that have not yet been produced to date.

Note added in proof. After this paper was submitted, a similar attempt to use GEMINI++ with TDHF results was posted on arXiv [100] by A.S. Umar, C. Simenel, and W. Ye, although the PNP method is not employed in their work.

ACKNOWLEDGMENTS

The author wishes to thank Kazuhiro Yabana (University of Tsukuba) for useful comments on this article. The author is grateful to Lorenzo Corradi (INFN-LNL) and Yutaka Watanabe (KEK-Japan) for providing the experimental data. Lu Guo (University of Chinese Academy of Sciences) is also thanked for useful information on GEMINI++. The author acknowledges support of Polish National Science Centre (NCN) Grant, Decision No. DEC-2013/08/A/ST3/00708. The author is grateful for continuous usage of computational resources of the HPCI system (HITACHI SR16000/M1) provided by Information Initiative Center (IIC), Hokkaido University, through the HPCI System Research Projects (Projects No. hp120204, No. hp140010, No. 150081, No. hp160062, and No. hp170007).

[1] A. Winther, Nucl. Phys. A **572**, 191 (1994); **594**, 203 (1995).
[2] E. Vigezzi and A. Winther, Ann. Phys. (NY) **192**, 432 (1989).
[3] L. Corradi, G. Pollarolo, and S. Szilner, J. Phys. G: Nucl. Part. Phys. **36**, 113101 (2009).
[4] R. Yanez and W. Loveland, Phys. Rev. C **91**, 044608 (2015).
[5] V. Zagrebaev and W. Greiner, J. Phys. G: Nucl. Part. Phys. **31**, 825 (2005).
[6] V. Zagrebaev and W. Greiner, J. Phys. G: Nucl. Part. Phys. **34**, 1 (2007).
[7] V. Zagrebaev and W. Greiner, J. Phys. G: Nucl. Part. Phys. **34**, 2265 (2007).
[8] V. Zagrebaev and W. Greiner, Phys. Rev. Lett. **101**, 122701 (2008).
[9] V. Zagrebaev and W. Greiner, Phys. Rev. C **78**, 034610 (2008).
[10] V. I. Zagrebaev and W. Greiner, Phys. Rev. C **87**, 034608 (2013).
[11] V. I. Zagrebaev, B. Fornal, S. Leoni, and W. Greiner, Phys. Rev. C **89**, 054608 (2014).
[12] J. S. Barrett, W. Loveland, R. Yanez, S. Zhu, A. D. Ayangeakaa, M. P. Carpenter, J. P. Greene, R. V. F. Janssens, T. Lauritsen, E. A. McCutchan, A. A. Sonzogni, C. J. Chiara, J. L. Harker, and W. B. Walters, Phys. Rev. C **91**, 064615 (2015).
[13] N. V. Antonenko, E. A. Cherepanov, A. K. Nasirov, V. P. Permjakov, and V. V. Volkov, Phys. Rev. C **51**, 2635 (1995).
[14] G. G Adamian, N. V. Antonenko, and W. Scheid, Nucl. Phys. A **618**, 176 (1997).
[15] G. G Adamian, N. V. Antonenko, W. Scheid, and V. V. Volkov, Nucl. Phys. A **627**, 361 (1997).
[16] G. G Adamian, N. V. Antonenko, W. Scheid, and V. V. Volkov, Nucl. Phys. A **633**, 409 (1998).
[17] G. G. Adamian, N. V. Antonenko, and W. Scheid, Phys. Rev. C **68**, 034601 (2003).
[18] Z.-Q. Feng, G.-M. Jin, and J.-Q. Li, Phys. Rev. C **80**, 067601 (2009).
[19] G. G. Adamian, N. V. Antonenko, V. V. Sargsyan, and W. Scheid, Phys. Rev. C **81**, 024604 (2010).
[20] G. G. Adamian, N. V. Antonenko, V. V. Sargsyan, and W. Scheid, Phys. Rev. C **81**, 057602 (2010).
[21] G. G. Adamian, N. V. Antonenko, and D. Lacroix, Phys. Rev. C **82**, 064611 (2010).
[22] M.-H. Mun, G. G. Adamian, N. V. Antonenko, Y. Oh, and Y. Kim, Phys. Rev. C **89**, 034622 (2014).
[23] M.-H. Mun, G. G. Adamian, N. V. Antonenko, Y. Oh, and Y. Kim, Phys. Rev. C **91**, 054610 (2015).
[24] L. Zhu, Z.-Q. Feng, and F. S. Zhang, J. Phys. G: Nucl. Part. Phys. **42**, 085102 (2015).
[25] Z.-Q. Feng, Phys. Rev. C **95**, 024615 (2017).
[26] L. Zhu, J. Su, and P.-W. Wen, Phys. Rev. C **95**, 044608 (2017).
[27] L. Zhu, J. Su, and F.-S. Zhang, Nucl. Phys. A **964**, 93 (2017).
[28] L. Zhu, J. Su, W.-J. Xie, and F.-S. Zhang, Phys. Lett. B **767**, 437 (2017).
[29] N. Wang, Z. Li, and X. Wu, Phys. Rev. C **65**, 064608 (2002).
[30] N. Wang, Z. Li, X. Wu, J. Tian, Y. Zhang, and M. Liu, Phys. Rev. C **69**, 034608 (2004).
[31] J. Tian, X. Wu, K. Zhao, Y. Zhang, and Z. Li, Phys. Rev. C **77**, 064603 (2008).
[32] K. Zhao, Z. Li, X. Wu, and Y. Zhang, Phys. Rev. C **88**, 044605 (2013).
[33] K. Zhao, Z. Li, N. Wang, Y. Zhang, Q. Li, Y. Wang, and X. Wu, Phys. Rev. C **92**, 024613 (2015).
[34] N. Wang, K. Zhao, and Z. Li, Science China Physics, Mechanics & Astronomy **58**, 112001 (2015).
[35] C. Li, F. Zhang, J. Li, L. Zhu, J. Tian, N. Wang, and F.-S. Zhang, Phys. Rev. C **93**, 014618 (2016).
[36] N. Wang, T. Wu, J. Zeng, Y. Yang, and L. Ou, J. Phys. G: Nucl. Part. Phys. **43**, 065101 (2016).
[37] K. Zhao, Z. Li, Y. Zhang, N. Wang, Q. Li, C. Shen, Y. Wang, and X. Wu, Phys. Rev. C **94**, 024601 (2016).
[38] H. Yao and N. Wang, Phys. Rev. C **95**, 014607 (2017).
[39] P. A. M. Dirac, Proc. Camb. Philos. Soc. **26**, 376 (1930).
[40] P. Bonche, S. Koonin, and J. W. Negele, Phys. Rev. C **13**, 1226 (1976).
[41] J. W. Negele, Rev. Mod. Phys. **54**, 913 (1982).
[42] C. Simenel, Eur. Phys. J. A **48**, 152 (2012).
[43] T. Nakatsukasa, Prog. Theor. Exp. Phys. (2012) 01A207.
[44] J. A. Maruhn, P.-G. Reinhard, P. D. Stevenson, and A. S. Umar, Comput. Phys. Commun. **185**, 2195 (2014).
[45] T. Nakatsukasa, K. Matsuyanagi, M. Matsuo, and K. Yabana, Rev. Mod. Phys. **88**, 045004 (2016).
[46] K. Sekizawa and K. Yabana, Phys. Rev. C **88**, 014614 (2013); **93**, 029902(E) (2016).
[47] K. Sekizawa and K. Yabana, Phys. Rev. C **90**, 064614 (2014).
[48] K. Sekizawa, Ph.D thesis, University of Tsukuba, 2015.
[49] Sonika, B. J. Roy, A. Parmar, U. K. Pal, H. Kumawat, V. Jha, S. K. Pandit, V. V. Parkar, K. Ramachandran, K. Mahata, A. Pal, S. Santra, A. K. Mohanty, and K. Sekizawa, Phys. Rev. C **92**, 024603 (2015).
[50] K. Sekizawa and K. Yabana, Phys. Rev. C **93**, 054616 (2016).

[51] K. Sekizawa and S. Heinz, Acta Phys. Pol. B Proc. Suppl. **10**, 225 (2017).
[52] C. Simenel, Phys. Rev. Lett. **105**, 192701 (2010).
[53] R. J. Charity, in *Joint ICTP-AIEA Advanced Workshop on Model Codes for Spallation Reactions*, Report INDC(NDC)-0530 (IAEA, Vienna, 2008), p. 139; The GEMINI++ code can be downloaded from https://bitbucket.org/arekfu/gemini.
[54] R. Balian and M. Véneroni, Phys. Rev. Lett. **47**, 1353 (1981).
[55] S. E. Koonin, K. T. R. Davies, V. Maruhn-Rezwani, H. Feldmeier, S. J. Krieger, and J. W. Negele, Phys. Rev. C **15**, 1359 (1977).
[56] K. T. R. Davies, V. Maruhn-Rezwani, S. E. Koonin, and J. W. Negele, Phys. Rev. Lett. **41**, 632 (1978).
[57] C. H. Dasso, T. Døssing, and H. C. Pauli, Z. Phys. A **289**, 395 (1979).
[58] C. Simenel, Phys. Rev. Lett. **106**, 112502 (2011).
[59] G. Scamps, D. Lacroix, G. F. Bertsch, and K. Washiyama, Phys. Rev. C **85**, 034328 (2012).
[60] G. Scamps and D. Lacroix, Phys. Rev. C **87**, 014605 (2013).
[61] S. Ebata and T. Nakatsukasa, JPS Conf. Proc. **1**, 013038 (2014).
[62] S. Ebata and T. Nakatsukasa, JPS Conf. Proc. **6**, 020056 (2015).
[63] Y. Hashimoto and G. Scamps, Phys. Rev. C **94**, 014610 (2016).
[64] P. Magierski, K. Sekizawa, and G. Wlazłowski, Phys. Rev. Lett. (to be published), arXiv:1611.10261.
[65] K. Sekizawa, P. Magierski, and G. Wlazlowski, Proceedings of Science **(INPC2016)** 214 (2017); arXiv:1702.0069.
[66] K. Sekizawa, G. Wlazlowski, and P. Magierski, EPJ Web of Conf. (to be published), arXiv:1705.4902.
[67] E. Chabanat, P. Bonche, P. Haensel, J. Meyer, and R. Schaeffer, Nucl. Phys. A **635**, 231 (1998); **643**, 441 (1998).
[68] R. J. Charity, M. A. McMahan, G. J. Wozniak, R. J. McDonald, L. G. Moretto, D. G. Sarantites, L. G. Sobotka, G. Guarino, A. Pantaleo, L. Fiore, A. Gobbi, and K. D. Hildenbrand, Nucl. Phys. A **483**, 371 (1988).
[69] W. Hauser and H. Feshbach, Phys. Rev. **87**, 366 (1952).
[70] L. G. Moretto, Nucl. Phys. A **247**, 211 (1975).
[71] N. Bohr and J. A. Wheeler, Phys. Rev. **56**, 426 (1939).
[72] R. J. Charity, Phys. Rev. C **82**, 014610 (2010).
[73] D. Mancusi, R. J. Charity, and J. Cugnon, Phys. Rev. C **82**, 044610 (2010).
[74] L. Corradi, J. H. He, D. Ackermann, A. M. Stefanini, A. Pisent, S. Beghini, G. Montagnoli, F. Scarlassara, G. F. Segato, G. Pollarolo, C. H. Dasso, and A. Winther, Phys. Rev. C **54**, 201 (1996).
[75] L. Corradi, A. M. Stefanini, J. H. He, S. Beghini, G. Montagnoli, F. Scarlassara, G. F. Segato, G. Pollarolo, and C. H. Dasso, Phys. Rev. C **56**, 938 (1997).
[76] S. Szilner, L. Corradi, G. Pollarolo, S. Beghini, B. R. Behera, E. Fioretto, A. Gadea, F. Haas, A. Latina, G. Montagnoli, F. Scarlassara, A. M. Stefanini, M. Trotta, A. M. Vinodkumar, and Y. Wu, Phys. Rev. C **71**, 044610 (2005).
[77] L. Corradi, A. M. Vinodkumar, A. M. Stefanini, E. Fioretto, G. Prete, S. Beghini, G. Montagnoli, F. Scarlassara, G. Pollarolo, F. Cerutti, and A. Winther, Phys. Rev. C **66**, 024606 (2002).
[78] L. Corradi, A. M. Stefanini, C. J. Lin, S. Beghini, G. Montagnoli, F. Scarlassara, G. Pollarolo, and A. Winther, Phys. Rev. C **59**, 261 (1999).
[79] Y. X. Watanabe, Y. H. Kim, S. C. Jeong, Y. Hirayama, N. Imai, H. Ishiyama, H. S. Jung, H. Miyatake, S. Choi, J. S. Song, E. Clement, G. de France, A. Navin, M. Rejmund, C. Schmitt, G. Pollarolo, L. Corradi, E. Fioretto, D. Montanari, M. Niikura, D. Suzuki, H. Nishibata, and J. Takatsu, Phys. Rev. Lett. **115**, 172503 (2015).
[80] H. Freiesleben and J. V. Kratz, Phys. Rep. **106**, 1 (1984).
[81] C.-C. Sahm, H.-G. Clere, K.-H. Schmidt, W. Reisdorf, P. Armbruster, F. P. Heßberger, J. G. Keller, G. Münzenberg, and D. Vermeulen, Z. Phys. A **319**, 113 (1984).
[82] GRAZING calculations can be performed online via the website of Nuclear Reactions Video (NRV) Project: http://nrv.jinr.ru/nrv/webnrv/grazing/; The default parameter set was used. Fine tuning of the model parameters may, to some extent, improve the description.
[83] K. Sekizawa and K. Yabana, EPJ Web of Conf. **86**, 00043 (2015).
[84] K. Sekizawa and K. Yabana, Multinucleon Transfer Reaction in Time-Dependent Hartree-Fock Theory, an invited paper honoring Prof. Joachim Maruhn's retirement to be published as a chapter in *Progress of Time-Dependent Nuclear Reaction Theory*, edited by Yoritaka Iwata, in the ebook series, "Frontiers in Nuclear and Particle Physics" (Bentham Science Publishers, Sharjah, 2017); arXiv:1511.08322.
[85] I. Dostrovsky, Z. Fraenkel, and G. Friedlander, Phys. Rev. **116**, 683 (1959); **119**, 2098 (1960).
[86] S. Ayik, Phys. Lett. B **658**, 174 (2008).
[87] Y. Tanimura, D. Lacroix, and S. Ayik, Phys. Rev. Lett. **118**, 152501 (2017).
[88] W. Shun-jin and W. Cassing, Ann. Phys. (NY) **159**, 328 (1985).
[89] M. Tohyama, Phys. Lett. B **160**, 235 (1985).
[90] M. Gong and M. Tohyama, Z. Phys. A **335**, 153 (1990).
[91] M. Tohyama and A. S. Umar, Phys. Rev. C **93**, 034607 (2016).
[92] J. F. Berger, M. Girod, and D. Gogny, Nucl. Phys. A **428**, 23c (1984).
[93] C. Simenel, J. Phys. G: Nucl. Part. Phys. **41**, 094007 (2014).
[94] T. Kato and H. Kono, Chem. Phys. Lett. **392**, 533 (2004).
[95] J. Caillat, J. Zanghellini, M. Kitzler, O. Koch, W. Kreuzer, and A. Scrinzi, Phys. Rev. A **71**, 012712 (2005).
[96] W. J. Huang, G. Audi, M. Wang, F. G. Kondev, S. Naimi, and X. Xu, Chin. Phys. C **41**, 030002 (2017).
[97] M. Wang, G. Audi, F. G. Kondev, W. J. Huang, S. Naimi, and X. Xu, Chin. Phys. C **41**, 030003 (2017).
[98] P. Möller, A. J. Sierk, T. Ichikawa, and H. Sagawa, At. Data Nucl. Data Tables **109-110**, 1 (2016).
[99] It was pointed out that an old version of the GRAZING code which is currently available on the NRV Web site [82] contains some error in evaluating evaporation effects around $A \approx 126$ that makes resulting cross sections look slightly awkward. It was corrected in the latest version of the GRAZING code http://personalpages.to.infn.it/nanni/grazing/. Therefore, the GRAZING results shown in Fig. 10 were also taken from Ref. [79]. I would like to thank Yutaka Watanabe for pointing it out to me.
[100] A. S. Umar, C. Simenel, and W. Ye, arXiv:1706.05024.